ELSEVIER

International Journal of Solids and Structures 41 (2004) 2189–2203

INTERNATIONAL JOURNAL OF SOLIDS and STRUCTURES

www.elsevier.com/locate/ijsolstr

Effects of thermal residual stresses on effective elastoplastic behavior of metal matrix composites

H.T. Liu, L.Z. Sun *

Department of Civil and Environmental Engineering and Center for Computer-Aided Design, The University of Iowa, Iowa City, IA 52242-1527, USA

Received 25 June 2002; received in revised form 20 August 2003

Abstract

During the fabrication processes of particle-reinforced metal-matrix composites, thermal residual stresses are normally developed due to the difference of the coefficients of thermal expansion between the matrix and the reinforcement. The effect of thermal residual stresses is analytically investigated on the elastoplastic behavior of the composites. Micromechanical stress and strain fields are calculated due to the combination of applied external loads and prescribed thermal mismatch eigenstrains. Ensemble-volume averaging procedures are then employed to derive the effective yield function of the composites. It is shown that the residual stresses result in a combined kinematic hardening and isotropic hardening effect. Comparisons between the analytical predictions and experimental data are performed to illustrate the capability of the proposed model.

Keywords: Metal-matrix composites; Micromechanics; Homogenization; Effective elastoplastic behavior; Thermal residual stress; Strain hardening

1. Introduction

Because of the improved stiffness and strength with lightweight compared with conventional metallic alloys, metal-matrix composites (MMCs) have the great potential to be applied in the aerospace, defense, and automotive industries. The mechanical properties of MMCs generally reflect the combination of those of the matrices and the reinforcements. Reinforcements may be continuous in the form of long fibers or discontinuous in the form of particulates, short fibers or whiskers. Particle-reinforced MMCs (PRMMCs) are less expensive to fabricate. They can be shaped by standard metallurgical processes such as forging, rolling, and extrusion.

Internal residual stresses in composites are the ones which remain stationary and at equilibrium with their surroundings. The mechanical performance of materials may be significantly affected. On the other

* Corresponding author. Tel.: +1-319-384-0830; fax: +1-319-335-5660.
E-mail address: lizhi-sun@uiowa.edu (L.Z. Sun).

0020-7683/$ - see front matter © 2003 Elsevier Ltd. All rights reserved.
doi:10.1016/j.ijsolstr.2003.11.038

hand, the existence of internal residual stresses may be beneficial if designed deliberately (Withers and Bhadeshia, 2001a,b). Therefore, it is important to quantitatively understand how residual stresses influence the mechanical responses of PRMMCs under external loading. During the fabrication and subsequent heat treatment processes, PRMMCs initially behave in a stress-free state at the solution treatment temperature and then develop significant thermal residual stresses upon cooling to the room temperature. This is due to the difference of coefficient of thermal expansion (CTE) between the matrix (e.g., CTE of Al: $\alpha_0 = 21.5 \times 10^{-6}/^{\circ}\mathrm{C}$) and the reinforcement (e.g., CTE of SiC: $\alpha_1 = 3.8 \times 10^{-6}/^{\circ}\mathrm{C}$). Since the CTE of the metallic matrix is greater than that of the ceramic particles, the matrix shrinks tight around the particles, resulting in the internal tensile stresses in the matrix and compressive stresses in the particles. The local plastic deformation may occur if the residual stresses exceed the yield strength of the matrix during the cooling process.

Various models have been developed to tackle the thermal residual stresses and their effect on the overall (effective) mechanical performance of unidirectionally aligned PRMMCs, either analytically (Arsenault and Taya, 1987; Withers et al., 1989; Dunn and Taya, 1994; Ramakrishnan, 1996; Hu and Weng, 1998; Jiang et al., 1998) or computationally (Povirk et al., 1991; Levy and Papazian, 1991; Zahl and McMeeking, 1991; Shi et al., 1992; Davis and Allison, 1993; Dutta et al., 1993; Ho and Saigal, 1994; Jain et al., 1994; Meijer et al., 2000; Teixeira-Dias and Menezes, 2001; Bruzzi et al., 2001). It is noted that both analytical and numerical treatments have their advantages and disadvantages (Dunn and Ledbetter, 1997). In general, analytical micromechanical approaches consider the analysis of a representative volume element (RVE) in which the reinforcement geometry is idealized for the ease of mathematical treatment. For example, reinforcing particles, short fibers, or whiskers are usually modeled by spheroids so that the celebrated Eshelby's equivalent inclusion theory (Eshelby, 1957, 1959) can be applied. Direct interactions between reinforcements are rarely taken into consideration. Most analytical approaches are directed toward random distribution of particles. Homogenized constitutive equations of composites are often derived in an explicit way so that they can be directly implemented for structural analysis.

On the other hand, most of computational micromechanics approaches are based on the periodic unit cell models, which have the advantage of high accuracy of solutions by considering realistic geometry of reinforcements and local interactions among reinforcements with the expense of intensive computational cost. Periodic boundary conditions introduce a periodicity in the reinforcement distribution that may not exist in actual composites. In addition, numerical models do not result in explicit forms for the overall constitutive relations, making them difficult to implement in stress analyses at the macroscopic level.

Recognizing each approach has its own advantages and disadvantages, the present paper seeks to apply an analytical micromechanics framework with prescribed thermal eigenstrains to tackle the effect of processing-induced residual stresses on the effective elastoplastic behavior of PRMMCs. Although previous investigations mentioned above have provided a significant understanding of the role of thermal residual stresses on the effective constitutive relations of composites, the results obtained are not quite consistent with each other and not systematic. Therefore, the present paper will perform a parametric study of how intrinsically residual stresses affect the overall uniaxial tensile/compressional yield strengths, multiaxial yield surfaces, and strain hardenings of unidirectionally aligned PRMMCs. Based on the very recent work of Ju and Sun (2001) and Sun and Ju (2001), micromechanical stress and strain fields are re-derived due to the combination of the prescribed eigenstrains (due to thermal mismatch of CTEs) and the equivalent eigenstrains (due to applied external loading). The ensemble-averaged homogenization procedure is utilized to derive the effective yield function of composites under general three-dimensional loading conditions. It is shown that the residual stresses result in a combined kinematic hardening and isotropic hardening effect. Comparisons between the analytical predictions and experimental data are performed to illustrate the capability of the proposed model.

2. Micromechanical framework and homogenization

Let us consider a particle-reinforced composite with a linearly elastic matrix (phase 0) and randomly dispersed yet unidirectionally aligned, linearly elastic spheroidal particles (phase 1) as shown in Fig. 1. Both the particles and the matrix are isotropic with the elastic stiffness tensors denoted by $\mathbf{C}^1$ and $\mathbf{C}^0$, and the CTEs designated as α_1 and α_0, respectively. The volume fraction of the particles is ϕ. The composite is subjected to a uniform temperature change ΔT, and after that, it is further subjected to a far-field mechanical stress $\boldsymbol{\sigma}_0$ (or the far-field strain $\boldsymbol{\varepsilon}_0$).

From concept of eigenstrains (Mura, 1987), the effects of the temperature change can be simulated by a prescribed uniform eigenstrain $\boldsymbol{\varepsilon}^*$ inside the particles that

$$\varepsilon^*_{ij} = (\alpha_1 - \alpha_0)\Delta T \delta_{ij} \tag{1}$$

Here, δ_{ij} is the second-rank identity tensor (Kronecker delta). If the temperature change is significant enough, the prescribed eigenstrain will cause the matrix yield and produce plastic flow. The overall elastoplastic behavior of PRMMCs depends on the collective responses of local stress field through the homogenization averaging procedure. For simplicity, the von Mises yield criterion with an isotropic hardening law is adopted for the matrix material.

To obtain the effective elastoplastic constitutive relations of PRMMCs, homogenization procedure is usually performed within a mesoscopic RVE (Nemat-Nasser and Hori, 1999). The microscopic stress $\boldsymbol{\sigma}(\mathbf{x})$ at a material point $\mathbf{x}$ is assumed to satisfy the von Mises yield criterion:

$$F(\boldsymbol{\sigma}, e^{\mathrm{p}}) = \sqrt{\boldsymbol{\sigma} : \mathbf{I}_{\mathrm{d}} : \boldsymbol{\sigma}} - K(e^{\mathrm{p}}) \leqslant 0 \tag{2}$$

where e^{p} and $K(e^{\mathrm{p}})$ are the equivalent plastic strain and the isotropic hardening function of the matrix, respectively. Moreover, $\mathbf{I}_{\mathrm{d}}$ denotes the deviatoric part of the fourth-rank identity tensor $\mathbf{I}$. The notation ":" indicates the tensor contraction between a fourth-rank tensor and a second-rank tensor.

The square of the "current stress norm" $H(\mathbf{x}|g) \triangleq \boldsymbol{\sigma}(\mathbf{x}|g) : \mathbf{I}_{\mathrm{d}} : \boldsymbol{\sigma}(\mathbf{x}|g)$ at a local point $\mathbf{x}$ is defined to contribute to the initial yield criterion of composites for a given particle configuration g (assembly) (Ju and Sun, 2001). Furthermore, $\langle H \rangle_{\mathrm{m}}(\mathbf{x})$ is designated as the ensemble average of $H(\mathbf{x}|g)$ over all possible

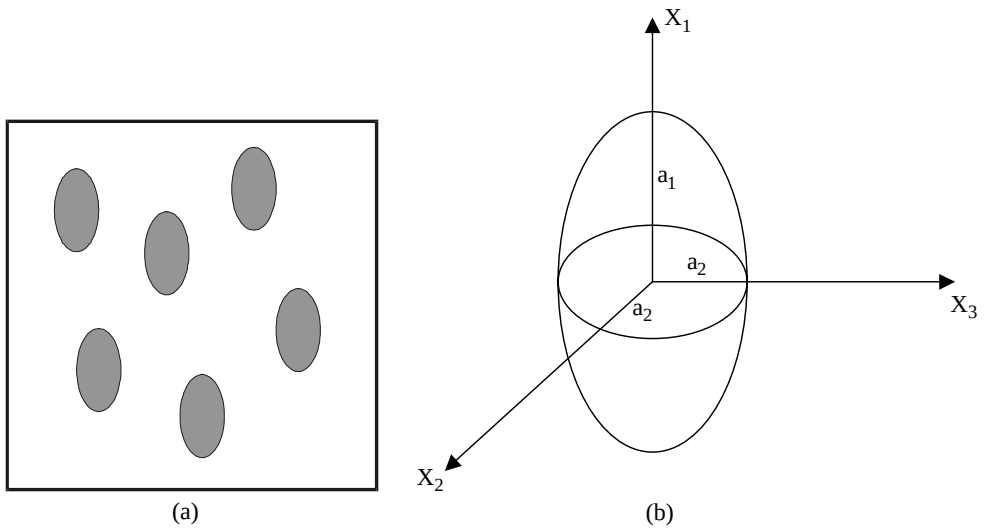

Fig. 1. Schematic diagram of (a) the microstructure of PRMMCs and (b) geometry of a spheroidal particle.

realizations for a matrix point $\mathbf{x}$. By neglecting the direct interactions among neighboring particles, $\langle H\rangle_{\mathrm{m}}(\mathbf{x})$ can be expressed as

$$\langle H\rangle_{\mathrm{m}}(\mathbf{x}) = H^0 + \frac{N}{V}\int_{\mathbf{x}'\notin\Xi(\mathbf{x})}[H(\mathbf{x}|\mathbf{x}') - H^0]\,\mathrm{d}\mathbf{x}' \tag{3}$$

if the aligned particles are uniformly distributed in the matrix. In above equation, $H^0 = \boldsymbol{\sigma}_0 : \mathbf{I}_{\mathrm{d}} : \boldsymbol{\sigma}_0$ is the square of the applied far-field stress norm and $\Xi(\mathbf{x})$ is the exclusion zone of $\mathbf{x}$ for the center location $\mathbf{x}'$ of a particle in the probability space, which is identical to the shape and size of a spheroidal particle. Furthermore, N and V are the number of particles in and the volume of the RVE, respectively.

At any point $\mathbf{x}$ in the matrix, the local stress $\boldsymbol{\sigma}(\mathbf{x})$ is the superposition of the far-field stress $\boldsymbol{\sigma}_0$ and the disturbed stress $\boldsymbol{\sigma}'(\mathbf{x})$:

$$\boldsymbol{\sigma}(\mathbf{x}) = \boldsymbol{\sigma}_0 + \boldsymbol{\sigma}'(\mathbf{x}) \tag{4}$$

where the disturbed stress $\boldsymbol{\sigma}'(\mathbf{x})$ is expressed as

$$\boldsymbol{\sigma}'(\mathbf{x}) = \mathbf{C}^0 : \overline{\mathbf{G}}(\mathbf{x} - \mathbf{x}_1) : \boldsymbol{\varepsilon}^{**} \tag{5}$$

in which $\overline{\mathbf{G}}$ is the exterior-point Eshelby's tensor (Ju and Sun, 1999) and $\boldsymbol{\varepsilon}^{**}$ is the total eigenstrain that includes the prescribed thermal eigenstrain $\boldsymbol{\varepsilon}^*$ and the equivalent eigenstrain induced by the far-field stresses:

$$\boldsymbol{\varepsilon}^{**} = (\mathbf{S} + \mathbf{A})^{-1} : (\mathbf{B} : \boldsymbol{\varepsilon}^* - \boldsymbol{\varepsilon}^0) \tag{6}$$

It is further noted that $\mathbf{S}$ is (interior-point) Eshelby tensor and $\mathbf{A}$ and $\mathbf{B}$ are the elastic mismatch fourth-rank tensors which render the following forms:

$$\mathbf{A} = (\mathbf{C}^1 - \mathbf{C}^0)^{-1} \cdot \mathbf{C}^0 \tag{7}$$

$$\mathbf{B} = (\mathbf{C}^1 - \mathbf{C}^0)^{-1} \cdot \mathbf{C}^1 \tag{8}$$

where the notation "$\cdot$" indicates the tensor contraction between two fourth-rank tensors.

From Eqs. (3)–(8), after a series of lengthy but straightforward derivations, the ensemble-averaged $\langle H\rangle_{\mathrm{m}}$ can be shown as

$$\langle H\rangle_{\mathrm{m}}(\mathbf{x}) = \boldsymbol{\sigma}_0 : \mathbf{I}_{\mathrm{d}} : \boldsymbol{\sigma}_0 + (\boldsymbol{\sigma}_0 - \mathbf{L} : \boldsymbol{\varepsilon}^*) : \mathbf{T} : (\boldsymbol{\sigma}_0 - \mathbf{L} : \boldsymbol{\varepsilon}^*) + 2(\mathbf{L} : \boldsymbol{\varepsilon}^*) : \mathbf{U} : (\boldsymbol{\sigma}_0 - \mathbf{L} : \boldsymbol{\varepsilon}^*) \tag{9}$$

where the fourth-rank tensors $\mathbf{T}$, $\mathbf{L}$ and $\mathbf{U}$ are defined as

$$T_{ijkl} = T^{(1)}_{IK}\delta_{ij}\delta_{kl} + T^{(2)}_{IJ}(\delta_{ik}\delta_{jl} + \delta_{il}\delta_{jk}) \tag{10}$$

$$\mathbf{L} = \mathbf{C}^0 \cdot \mathbf{B} \tag{11}$$

$$\mathbf{U} = (\mathbf{I}_{\mathrm{d}} \cdot \mathbf{C}^0) \cdot \mathbf{M} \cdot [\mathbf{C}^0 \cdot (\mathbf{A} + \mathbf{S})]^{-1} \tag{12}$$

with

$$T_{IK}^{(1)} = \frac{6(35v_0^2 - 70v_0 + 36)\Delta_{IK} + 14(50v_0^2 - 59v_0 + 8)(\Delta_I + \Delta_K) - 4(175v_0^2 - 343v_0 + 103)}{4725(1 - v_0)^2}\frac{\phi}{B_{II}B_{KK}} + \frac{2(25v_0 - 2)(1 - 2v_0)}{225(1 - v_0)^2}\frac{\phi(\Gamma_{II} + \Gamma_{KK})}{B_{II}B_{KK}} + \frac{2(25v_0 - 23)(1 - 2v_0)}{225(1 - v_0)^2}\frac{\phi(\Gamma_{II}\Delta_K + \Gamma_{KK}\Delta_I)}{B_{II}B_{KK}} + \frac{2(1 - 2v_0)^2}{3(1 - v_0)^2}\frac{\phi\Gamma_{II}\Gamma_{KK}}{B_{II}B_{KK}}$$

$$T_{IJ}^{(2)} = \frac{4(35v_0^2 - 70v_0 + 36)\Delta_{IJ} - (175v_0^2 - 266v_0 + 75)(\Delta_I + \Delta_J) + 4(175v_0^2 - 238v_0 + 82)}{3150(1 - v_0)^2}\frac{\phi}{B_{II}B_{JJ}} \tag{13}$$

$$M_{IJ}^{(1)} = M_{IJ}^{(2)} = \frac{\phi(3 + 7\Delta_{IJ} - 5(\Delta_I + \Delta_J))}{20(1 - v_0)} \tag{14}$$

Here, v_0 is the Possion's ratio of the matrix. Other parameters in the above equations are given in Appendix A.

Furthermore, from Ju and Chen (1994), the corresponding macroscopic (overall) stresses $\bar{\boldsymbol{\sigma}}$ produced by the far-field stress $\boldsymbol{\sigma}_0$ and the prescribed eigenstrain $\boldsymbol{\varepsilon}^*$ can be easily obtained as

$$\bar{\boldsymbol{\sigma}} = \mathbf{P} : \boldsymbol{\sigma}_0 + \mathbf{Q} : \boldsymbol{\varepsilon}^* \tag{15}$$

where the fourth-rank tensor $\mathbf{P}$ and $\mathbf{Q}$ read

$$\mathbf{P} = \mathbf{C}^0 \cdot [\mathbf{I} + \phi(\mathbf{I} - \mathbf{S}) \cdot (\mathbf{A} + \mathbf{S})^{-1}] \cdot (\mathbf{C}^0)^{-1} \tag{16}$$

$$\mathbf{Q} = \mathbf{C}^0 \cdot \phi(\mathbf{I} - \mathbf{S}) \cdot (\mathbf{A} + \mathbf{S})^{-1} \cdot \mathbf{B} \tag{17}$$

The combination of Eqs. (9) and (15) provides the expression of $\langle H \rangle_{\mathrm{m}}$ in terms of the overall stress tensor $\bar{\boldsymbol{\sigma}}$ and the prescribed eigenstrain tensor $\boldsymbol{\varepsilon}^*$.

3. Effective constitutive modeling of composites

With small deformation assumption, the macroscopic strain $\bar{\boldsymbol{\varepsilon}}$ can be directly decomposed into elastic part $\bar{\boldsymbol{\varepsilon}}^{\mathrm{e}}$ and plastic part $\bar{\boldsymbol{\varepsilon}}^{\mathrm{p}}$. The thermal residual stresses do not affect the elastic properties of composites. Therefore, Ju and Sun's (2001) effective elastic stiffness tensor $\overline{\mathbf{C}}$ for aligned spheroidal PRMMCs is still available for the composites with thermal residual stresses and is expressed as

$$\overline{\mathbf{C}} = \mathbf{C}^0 \cdot \{\mathbf{I} - \phi[-\mathbf{A} - (1 - \phi)\mathbf{S}]^{-1}\} \tag{18}$$

which shows the transversely isotropic behavior.

The overall plastic responses of the composites depend on the elastoplastic properties of the matrix. Isotropic strain-hardening law of the matrix has been adopted as

$$K(e^{\mathrm{p}}) = \sqrt{\tfrac{2}{3}}[\sigma_y + h(e^{\mathrm{p}})^q] \tag{19}$$

where σ_y, h and q are the yield stress and the strain-hardening parameters of the matrix, respectively. The overall plastic yield function of the composites is derived by applying the ensemble- and volume-average

procedures to the micromechanical yield function of the matrix Eq. (2). From the homogenization process in the previous section, the overall yield function of the composites can be expressed as

$$\overline{F} = (1-\phi)\sqrt{\langle H\rangle_{\mathrm{m}}} - \sqrt{\tfrac{2}{3}}[\sigma_y + h(\bar{e}^{\mathrm{p}})^q] \tag{20}$$

Here, $\bar{e}^{\mathrm{p}}$ is the overall equivalent plastic strain of the composites, defined as $\bar{e}^{\mathrm{p}} = \sqrt{2\bar{\boldsymbol{\varepsilon}}^{\mathrm{p}} : \bar{\boldsymbol{\varepsilon}}^{\mathrm{p}}/3}$. Correspondingly, the overall yield function is further applied to define the plastic associate flow rule between the effective plastic strain tensor and overall stress tensor of the composites:

$$\dot{\bar{\boldsymbol{\varepsilon}}}^{\mathrm{p}} = \dot{\lambda}\frac{\partial \overline{F}}{\partial \bar{\boldsymbol{\sigma}}} \tag{21}$$

where $\dot{\lambda}$ is the plastic consistency parameter, satisfying the Kuhn–Tucker conditions (Lubliner, 1990)

$$\dot{\lambda} \geqslant 0, \qquad \overline{F} \leqslant 0, \qquad \dot{\lambda}\overline{F} = 0, \qquad \dot{\lambda}\dot{\overline{F}} = 0 \tag{22}$$

Therefore, the complete plastic deformation framework is established via Eqs. (20) and (21).

4. Effects of thermal residual stresses

Due to the presence of the thermal residual stresses in PRMMCs, the overall elastoplastic behavior may exhibit differently from that without residual stresses in the composites. Based on the framework established above, the effect of thermal residual stresses on the overall elastoplastic deformation of PRMMCs is discussed in this section.

4.1. Cooling process

In the absence of external stresses ($\boldsymbol{\sigma}_0 = 0$), $\langle H\rangle_{\mathrm{m}}$ from Eq. (9) is simplified as

$$\langle H\rangle_{\mathrm{m}}(\mathbf{x}) = \boldsymbol{\varepsilon}^* : \overline{\mathbf{U}} : \boldsymbol{\varepsilon}^* \tag{23}$$

where

$$\overline{\mathbf{U}} = \mathbf{L}\cdot(\mathbf{T} - 2\mathbf{U})\cdot\mathbf{L} \tag{24}$$

and the prescribed thermal eigenstrain $\boldsymbol{\varepsilon}^*$ is defined in Eq. (1). It is noted that, if the temperature drop is large enough, the thermal residual stresses may cause the composites yield. The critical temperature drop ΔT^{c} that produces the composite initial yielding can be calculated by applying $\overline{F} = 0$ in Eq. (20) with $\bar{e}^{\mathrm{p}} = 0$.

The influence of the cooling process on the following mechanical responses of PRMMCs under external loading is characterized by the pre-stored thermal residual stresses in the composites. Corresponding to the given temperature drop and the prescribed eigenstrains $\boldsymbol{\varepsilon}^*$, the macroscopic averaged stresses $\bar{\boldsymbol{\sigma}}$ are expressed as Eq. (15) without external loading ($\boldsymbol{\sigma}_0 = 0$). To account for the change of matrix constraints to particles due to plastic flow, the secant moduli method (Berveiller and Zaoui, 1979; Tandon and Weng, 1998) is applied so that the Young's modulus E_0^{S} and Poisson's ratio v_0^{S} of the matrix are modified to become dependent on the equivalent plastic strain as

$$E_0^{\mathrm{S}} = \frac{1}{\frac{1}{E_0} + \frac{\bar{e}^{\mathrm{p}}}{\sigma_y + h(\bar{e}^{\mathrm{p}})^q}} \tag{25}$$

$$v_0^{\mathrm{S}} = \frac{1}{2} - \left(\frac{1}{2} - v_0\right)\frac{E_0^{\mathrm{S}}}{E_0} \tag{26}$$

The corresponding secant elastic stiffness tensor of the matrix is represented by $(\mathbf{C}^0)^{\mathrm{S}}$. Therefore, the thermal residual stresses $\bar{\boldsymbol{\sigma}}^{\mathrm{T}}$ caused by the temperature drop can be calculated by

$$\bar{\boldsymbol{\sigma}}^{\mathrm{T}} = \mathbf{Q}^{\mathrm{S}} : \boldsymbol{\varepsilon}^{*} \tag{27}$$

where $\mathbf{Q}^{\mathrm{S}}$ has the same expression as $\mathbf{Q}$ with the condition that $\mathbf{C}^{0}$ be replaced by $(\mathbf{C}^{0})^{\mathrm{S}}$.

In what follows, unless noted otherwise during subsequent numerical simulations, the matrix material is taken as an aluminum alloy with the Young's modulus $E_{\mathrm{m}} = 73$ GPa, Poisson's ratio $\nu_{\mathrm{m}} = 0.33$, the uniaxial yield strength $\sigma_y = 170$ MPa, the strain hardening parameters $h = 577$ MPa and $q = 0.37$, and the CTE $\alpha_0 = 21.5 \times 10^{-6}$ °C. For the elastic reinforcement material, the Young's modulus $E_{\mathrm{p}} = 480$ GPa, the Poisson's ratio $\nu_{\mathrm{p}} = 0.17$, and the CTE $\alpha_1 = 3.8 \times 10^{-6}$ °C (similar to the thermal-elastic properties of the

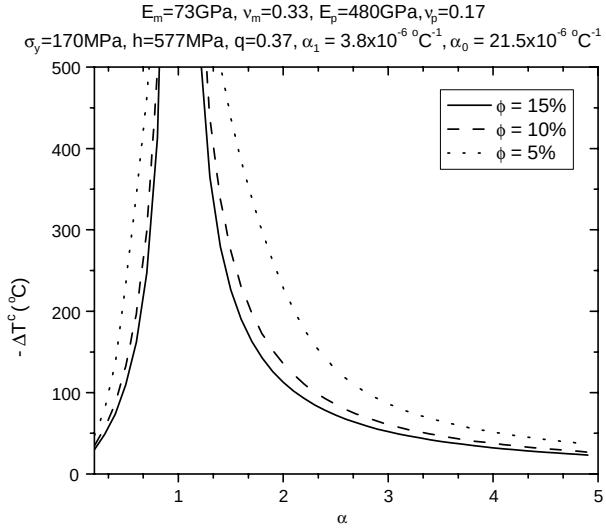

Fig. 2. The effect of aspect ratio on the critical temperature drop.

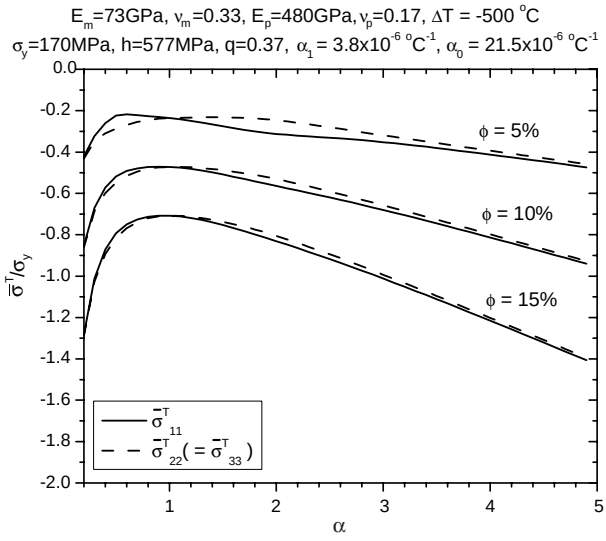

Fig. 3. Dependence of overall thermal residual stresses on the aspect ratio and volume fraction of particles.

SiC particles). Fig. 2 shows the critical temperature drop to produce initial yield of PRMMCs. The critical temperature drop increases rapidly when the particle aspect ratio α approaches to 1 (spherical particles), which indicates that the plastic flow is very difficult to occur in spherical PRMMCs. It is due to the fact that the local matrix material of spherical PRMMCs, under the pressure-independent von Mises yield criterion, is subjected to the purely hydrostatic stresses. Correspondingly, when the reinforcement concentration becomes less, it is even more difficult to yield. If the temperature drop is fixed at 500 °C (typical temperature for composites fabrication processing), the overall stress components acting on the composites are illustrated in Fig. 3. It is shown that all three normal stresses are compressive. The magnitude of each stress component increases with more particle concentration while the dependence of overall stresses on particle geometry is not monotonic.

4.2. Far-field mechanical loading

With the subsequent far-field mechanical loading $\boldsymbol{\sigma}_0$, $\langle H\rangle_{\mathrm{m}}$ inside the overall yield function Eq. (20) can be rewritten to explicitly take into account the overall thermal residual stresses $\bar{\boldsymbol{\sigma}}^{\mathrm{T}}$:

$$\langle H\rangle_{\mathrm{m}}(\mathbf{x}) = (\bar{\boldsymbol{\sigma}} + \bar{\boldsymbol{\sigma}}^{\mathrm{T}}) : \overline{\mathbf{T}} : (\bar{\boldsymbol{\sigma}} + \bar{\boldsymbol{\sigma}}^{\mathrm{T}}) \tag{28}$$

where

$$\overline{\mathbf{T}} = \mathbf{P}^{-1} \cdot (\mathbf{T} + \mathbf{I}_{\mathrm{d}}) \cdot \mathbf{P}^{-1} \tag{29}$$

Therefore, the overall yield function of PRMMCs becomes

$$\overline{F} = (1-\phi)\sqrt{(\bar{\boldsymbol{\sigma}} + \bar{\boldsymbol{\sigma}}^{\mathrm{T}}) : \overline{\mathbf{T}} : (\bar{\boldsymbol{\sigma}} + \bar{\boldsymbol{\sigma}}^{\mathrm{T}})} - \sqrt{\tfrac{2}{3}}[\sigma_y + h(\bar{e}^{\mathrm{p}}_{\mathrm{m}})^q] \tag{30}$$

The effect of thermal residual stresses on the overall uniaxial yield strength of PRMMCs is demonstrated in Figs. 4 and 5. Based on the fact of compressive residual stresses (Fig. 3), the tensile yield strength of PRMMCs is normally greater than the compressive yield strength, and both strengths are less than that without thermal residual stresses, regardless of aspect ratio and volume fraction of particles. Furthermore,

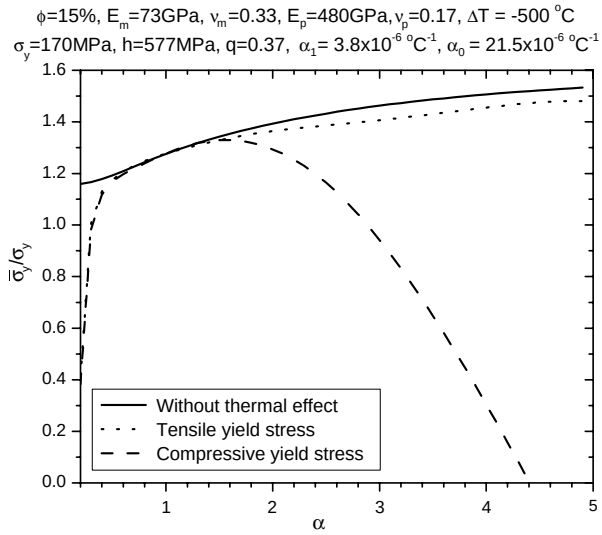

Fig. 4. The effect of aspect ratio on the yield stresses of the uniaxial loading.

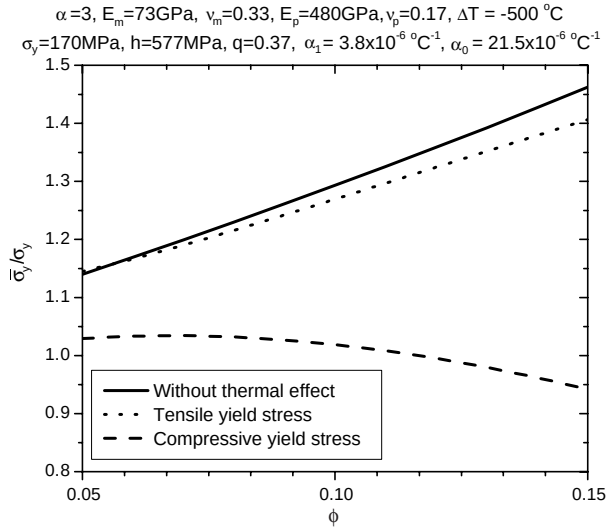

Fig. 5. The effect of particle volume fraction on the yield stresses of the uniaxial loading.

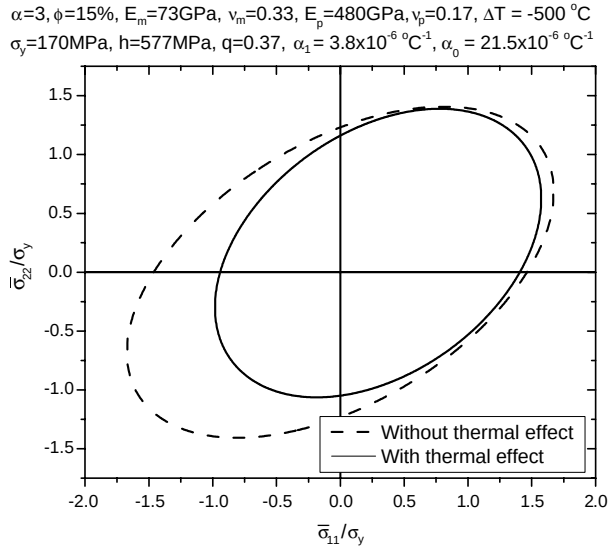

Fig. 6. The kinematic and isotropic hardening of the initial yield surface.

Fig. 4 illustrates that, with a large aspect ratio, the compressive strength could be zero, indicating that there is no elastic region for further compression. On the other hand, when particles are spherical, both tensile and compressive strengths are not affected by the internal thermal stresses. As shown in Fig. 5, the strength difference becomes more significant when the volume fraction of particles increases.

Thermal effects on the yield surfaces of PRMMCs under biaxial loading are investigated in Figs. 6–8. It is observed in Fig. 6 that the overall yield surface is a combination of *isotropic* and *kinematic* hardening responses under the consideration of thermal residual stresses whereas the yield surface without residual stresses shows isotropic hardening only. Fig. 7 further shows the effect of aspect ratio on the yield surfaces.

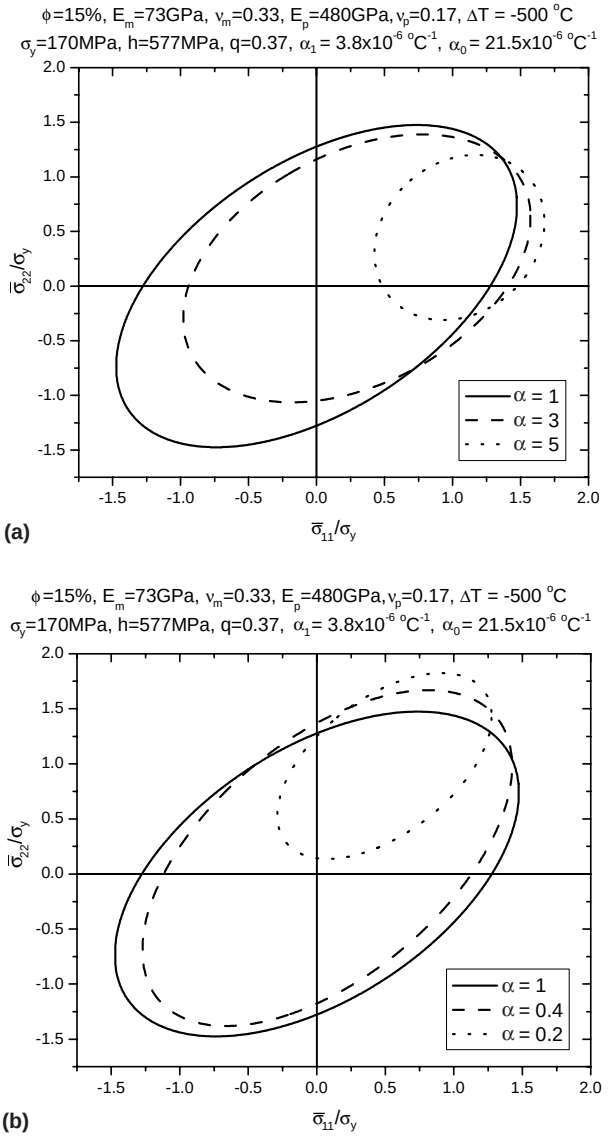

Fig. 7. The effect of aspect ratio on the initial yield surface (a) $\alpha > 1$ and (b) $\alpha < 1$.

When reinforcing spheroidal particles become more prolate (α increases from 1 to 5), the yield surfaces shrink and move toward the direction of particle alignment. On the other hand, when spheroidal particles become more (α decreases from 1 to 0.2), the yield surfaces shrink and move to the transverse direction of particle alignment where $\bar{\sigma}_{22}$ is applied. The reason for this phenomenon is that aspect ratios of reinforcement cause the composite stiffness anisotropic, which further affects the thermal stress distribution in PRMMCs. The effect of volume fraction of particles on the overall yield surface is illustrated in Fig. 8. With the increase of volume fraction, the yield surface exhibits more kinematic and moves toward the tensile loading directions.

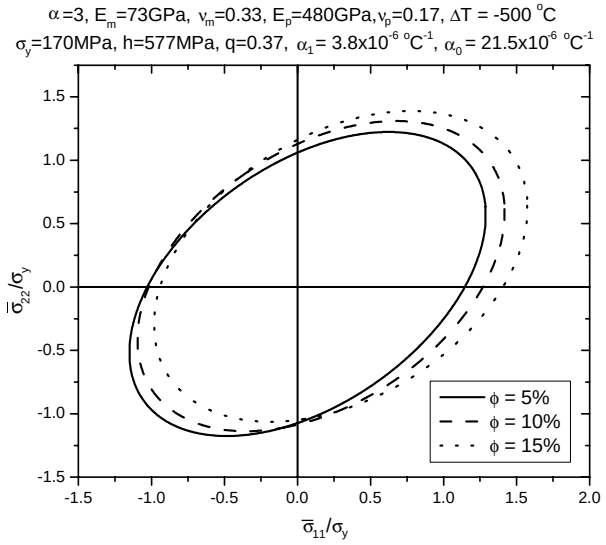

Fig. 8. The effect of volume fraction on the initial yield surface.

To investigate the influence of thermal residual stresses on the subsequent plastic flow of PRMMCs, uniaxial loading tests following the 500 °C temperature drop process have been considered; namely

$$\bar{\sigma}_{11} = \sigma > 0, \quad \text{other } \bar{\sigma}_{ij} = 0 \tag{31}$$

Fig. 9 shows the overall elastoplastic stress–strain relations of PRMMCs under a tension–compression loading process. With the consideration of thermal residual stresses, both the tensile and compressive plastic flow stresses become less than those without thermal effect. However, the overall stress–strain curves

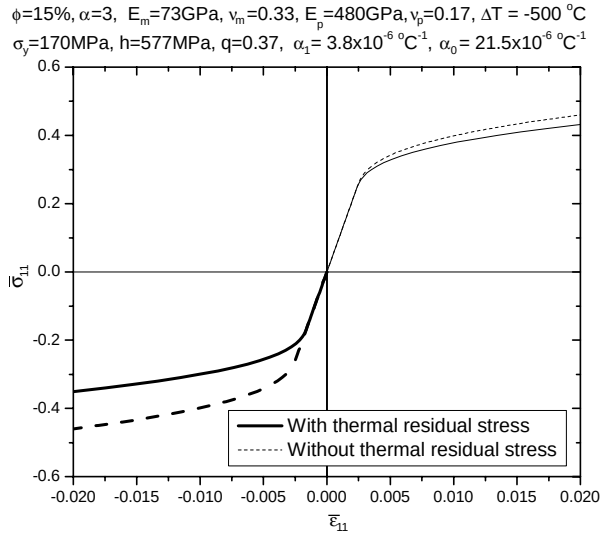

Fig. 9. Uniaxial loading: tension–compression curves.

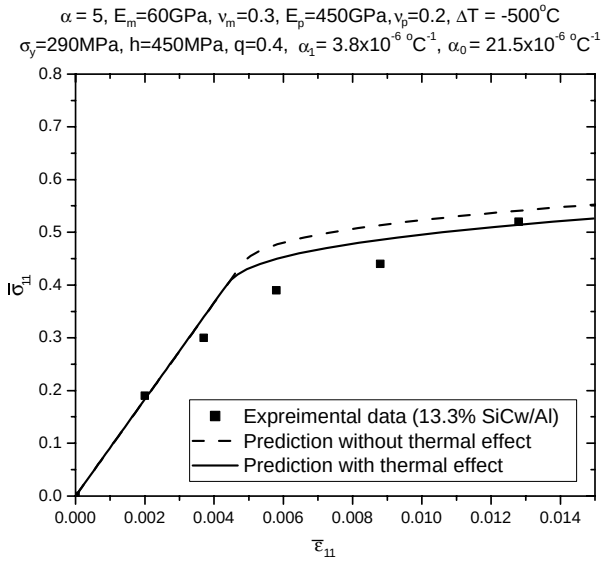

Fig. 10. Comparisons of uniaxial stress–strain responses with experimental data (Christman et al., 1989) for SiC_w/Al composites.

for tension and compression are not symmetric. Thermal stresses have a more significant effect on the compression part. Fig. 10 shows the comparison between the present predictions and the experimental data reported by Christman et al. (1989). In their experiments, uniaxial elastoplastic stress–strain curves were recorded for the 2124 aluminum alloy reinforced with 13.2% SiC whiskers. It is shown that the thermal residual stresses cause the overall elastoplastic stress–strain curve lower than that without thermal effects, which turns out the predication closer to the experimental data and therefore improves the accuracy of predications compared with the model without considering the thermal residual stresses.

5. Conclusions

A micromechanics-based elastoplastic model is developed to consider how processing-induced thermal residual stresses affect the overall mechanical behavior of PRMMCs. Micromechanical stress and strain fields are calculated due to the combination of applied external loads and prescribed thermal mismatch eigenstrains. Ensemble-volume averaging procedures are then employed to derive the effective yield function of the composites. The proposed effective elastoplastic constitutive model is suitable for general 3-D loading conditions. It is shown that the fabrication cooling process may cause plastic flow of the composites. Due to the presence of thermal residual stresses, the overall yield surfaces of the composites exhibit a combination of kinematic and isotropic plastic hardening even though the matrix material is assumed to be isotropic hardening only. Comparisons between the analytical predictions and experimental data are performed to illustrate the capability of the proposed model.

Acknowledgements

This work is sponsored by the Iowa Space Grant Consortium and the National Science Foundation (CMS-0084629).

Appendix A

Parameters in Eqs. (13) and (14) are expressed as

$$\begin{aligned}
&\Delta_1 = \frac{3[1-\alpha^4 f(\alpha^2)]}{1-\alpha^4}, \qquad \Delta_2 = \Delta_3 = \frac{1}{2}(3-\Delta_1)\\
&\Delta_{11} = \frac{5[2+\alpha^4-3\alpha^4 f(\alpha^2)]}{2(1-\alpha^4)^2}\\
&\Delta_{12} = \Delta_{21} = \Delta_{13} = \Delta_{31} = \frac{15\alpha^4[-3+(1+2\alpha^4)f(\alpha^2)]}{4(1-\alpha^4)^2}\\
&\Delta_{22} = \Delta_{23} = \Delta_{32} = \Delta_{33} = \frac{1}{8}(15-3\Delta_{11}-4\Delta_{12})
\end{aligned} \tag{A.1}$$

with $\alpha = a_1/a_2$ as the aspect ratio of the spheroidal particles (Fig. 1(b)) and

$$f(\alpha) = \begin{cases} \dfrac{\cos^{-1}\alpha}{\alpha\sqrt{1-\alpha^2}}, & \alpha < 1 \\ \dfrac{\cosh^{-1}\alpha}{\alpha\sqrt{\alpha^2-1}}, & \alpha > 1 \end{cases} \tag{A.2}$$

Further,

$$B_{IJ} = 2(V_{IJ} + N_{IJ}) \tag{A.3}$$

$$\begin{Bmatrix} \Gamma_{I1} \\ \Gamma_{I1} \\ \Gamma_{I1} \end{Bmatrix} = \begin{bmatrix} U_{11}+2V_{11}+M_{11}+2N_{11} & U_{21}+M_{21} & U_{31}+M_{31} \\ U_{12}+M_{12} & U_{22}+2V_{22}+M_{22}+2N_{22} & U_{32}+M_{32} \\ U_{13}+M_{13} & U_{23}+M_{23} & U_{33}+2V_{33}+M_{33}+2N_{33} \end{bmatrix}^{-1} \begin{Bmatrix} U_{I1}+M_{I1} \\ U_{I2}+M_{I2} \\ U_{I3}+M_{I3} \end{Bmatrix} \quad (I = 1,2,3) \tag{A.4}$$

with

$$\begin{aligned}
&U_{11} = \left[4v_0 + \frac{2}{\alpha^2-1}\right]h(\alpha) + 4v_0 + \frac{4}{3(\alpha^2-1)}\\
&U_{12} = U_{13} = \left[4v_0 - \frac{2\alpha^2+1}{\alpha^2-1}\right]h(\alpha) + 4v_0 - \frac{2\alpha^2}{\alpha^2-1}\\
&U_{21} = U_{31} = \left[-2v_0 - \frac{2\alpha^2+1}{\alpha^2-1}\right]h(\alpha) - \frac{2\alpha^2}{\alpha^2-1}\\
&U_{22} = U_{23} = U_{32} = U_{33} = \left[-2v_0 + \frac{4\alpha^2-1}{4(\alpha^2-1)}\right]h(\alpha) + \frac{\alpha^2}{2(\alpha^2-1)}
\end{aligned} \tag{A.5}$$

$$\begin{aligned}
&V_{11} = \left[-4v_0 + \frac{4\alpha^2-2}{\alpha^2-1}\right]h(\alpha) - 4v_0 + \frac{12\alpha^2-8}{3(\alpha^2-1)}\\
&V_{12} = V_{21} = V_{13} = V_{31} = \left[-v_0 - \frac{\alpha^2+2}{\alpha^2-1}\right]h(\alpha) - 2v_0 - \frac{2}{\alpha^2-1}\\
&V_{22} = V_{23} = V_{32} = V_{33} = \left[2v_0 - \frac{4\alpha^2-7}{4(\alpha^2-1)}\right]h(\alpha) + \frac{\alpha^2}{2(\alpha^2-1)}
\end{aligned} \tag{A.6}$$

$$M_{IJ} = \frac{\lambda^0\mu^1 - \lambda^1\mu^0}{(\mu^1 - \mu^0)[2(\mu^1 - \mu^0) + 3(\lambda^1 - \lambda^0)]}$$
$$N_{IJ} = \frac{\mu^0}{2(\mu^1 - \mu^0)} \tag{A.7}$$

and

$$h(\alpha) = \begin{cases} \dfrac{\alpha}{(1-\alpha^2)^{3/2}}[\alpha(1-\alpha^2)^{1/2} - \cos^{-1}\alpha], & \alpha < 1 \\ \dfrac{\alpha}{(\alpha^2-1)^{3/2}}[\cosh^{-1}\alpha - \alpha(\alpha^2-1)^{1/2}], & \alpha > 1 \end{cases} \tag{A.8}$$

It is noted that (λ^0, μ^0) and (λ^1, μ^1) are the Lame constants of the matrix and the particles, respectively.

References

Arsenault, R.J., Taya, M., 1987. Thermal residual stress in metal matrix composites. Acta Metall. 35, 651–659.

Berveiller, M., Zaoui, A., 1979. An extension of the self-consistent scheme to plastically flowing polycrystals. J. Mech. Phys. Solids 26, 325–344.

Bruzzi, M.S., McHugh, P.E., O'Rourke, F., Linder, T., 2001. Micromechanical modeling of the static and cyclic loading of an 2124-SiC MMC. Int. J. Plast. 17, 565–599.

Christman, T., Needleman, A., Suresh, S., 1989. An experimental and numerical study of deformation in metal-ceramic composites. Acta Metall. 37, 3029–3050.

Davis, L.C., Allison, J.E., 1993. Residual stresses and their effects on deformation in particle-reinforced metal-matrix composites. Metall. Trans. A 24, 2487–2496.

Dunn, M.L., Ledbetter, H., 1997. Elastic–plastic behavior of textured short-fiber composites. Acta Mater. 45, 3327–3340.

Dunn, M.L., Taya, M., 1994. Elastic–plastic thermal-stresses and deformation of short-fiber composites. J. Mater. Sci. 29, 2053–2062.

Dutta, I., Sims, J.D., Seigenthaler, D.M., 1993. An analytical study of residual stress effects on uniaxial deformation of whisker reinforced metal-matrix composites. Acta Metall. Mater. 41, 885–908.

Eshelby, J.D., 1957. The determination of the elastic field of an ellipsoidal inclusion and related problems. Proc. R. Soc. London, Ser. A 241, 376–396.

Eshelby, J.D., 1959. The elastic field outside an ellipsoidal inclusion. Proc. R. Soc. London, Ser. A 252, 561–569.

Ho, S., Saigal, A., 1994. Three-dimensional modeling of thermal residual stresses and mechanical behavior of cast SiC/Al particulate composites. Acta Metall. Mater. 42, 3253–3262.

Hu, G.K., Weng, G.J., 1998. Influence of thermal residual stresses on the composite macroscopic behavior. Mech. Mater. 27, 229–240.

Jain, M., MacEwan, S.R., Wu, L., 1994. Finite-element modeling of residual-stresses and strength differential effect in discontinuously reinforced metal-matrix composites. Mater. Sci. Eng. A 183, 111–120.

Jiang, Z., Lian, J., Yang, D., Dong, S., 1998. An analytical study of the influence of thermal residual stresses on the elastic and yield behaviors of short fiber-reinforced metal matrix composites. Mater. Sci. Eng. A 248, 256–275.

Ju, J.W., Chen, T.M., 1994. Micromechanics and effective moduli of elastic composites containing randomly dispersed ellipsoidal inhomogeneities. Acta Mech. 103, 103–121.

Ju, J.W., Sun, L.Z., 1999. A novel formulation for exterior-point Eshelby's tensor of an ellipsoidal inclusion. ASME J. Appl. Mech. 66, 570–574.

Ju, J.W., Sun, L.Z., 2001. Effective elastoplastic behavior of metal matrix composites containing randomly located aligned spheroidal inhomogeneities, Part I: micromechanics-based formulation. Int. J. Solids Struct. 38, 183–201.

Levy, A., Papazian, J.M., 1991. Elastoplastic finite element analysis of short-fiber-reinforced SiC/Al composites: effects of thermal treatment. Acta Metall. Mater. 39, 2255–2266.

Lubliner, J., 1990. Plasticity Theory. Macmillan Publishing Company.

Meijer, G., Ellyin, F., Xia, Z., 2000. Aspects of residual stress/strain in particle reinforced metal matrix composites. Composites Part B 31, 29–37.

Mura, T., 1987. Micromechanics of Defects in Solids, second ed. Kluwer Academic Publishers.

Nemat-Nasser, S., Hori, M., 1999. Micromechanics: Overall Properties of Heterogeneous Materials, second ed. North-Holland.

Povirk, G.L., Needleman, A., Nutt, S.R., 1991. An analysis of the effect of residual stresses on deformation and damage mechanisms in Al–SiC composites. Mater. Sci. Eng. A 132, 31–38.

Ramakrishnan, N., 1996. An analytical study on strengthening of particulate reinforced metal matrix composites. Acta Mater. 44, 69–77.

Shi, N., Wilner, B., Arsenault, R.J., 1992. An FEM study of the plastic deformation process of whisker reinforced SiC/Al composites. Acta Metall. Mater. 40, 2841–2854.

Sun, L.Z., Ju, J.W., 2001. Effective elastoplastic behavior of metal matrix composites containing randomly located aligned spheroidal inhomogeneities, Part II: applications. Int. J. Solids Struct. 38, 203–225.

Tandon, G.P., Weng, G.J., 1998. A theory of particle-reinforced plasticity. ASME J. Appl. Mech. 55, 126–135.

Teixeira-Dias, F., Menezes, L.F., 2001. Numerical aspects of finite element simulations of residual stresses in metal matrix composites. Int. J. Numer. Methods Eng. 50, 629–644.

Withers, P.J., Bhadeshia, H.K.D.H., 2001a. Residual stress, Part 1: measurement techniques. Mater. Sci. Technol. 17, 355–365.

Withers, P.J., Bhadeshia, H.K.D.H., 2001b. Residual stress, Part 2: nature and origins. Mater. Sci. Technol. 17, 366–375.

Withers, P.J., Stobbs, W.M., Pedersen, O.B., 1989. The application of the Eshelby method of internal stress determination to short fibre metal matrix composites. Acta Metall. 37, 3061–3084.

Zahl, D.B., McMeeking, R.M., 1991. The influence of residual stress on the yielding of metal matrix composites. Acta Metall. Mater. 39, 1117–1122.